Technical Note

Planar Nozzles for Controllable Microthrusters

P. H. Pedreira[1]; J. R. Lauretta[2]; and S. D'hers[3]

Abstract: Orbital maneuvering of microsatellite and nanosatellite requirements can be efficiently addressed by planar nozzles, in which real-time thrust control is gained actuating on the nozzle throat area. In the present work, the method of characteristics is used to design a hypersonic contour; then, the resulting profile is laser cut, assembled, and built into a propulsion system to finally perform tests in a vacuum chamber under several working conditions. Results are used to validate the profile and modeling assumptions and investigate overall behavior. Tests showed that thrust-inlet pressure ratio is a linear function of separation between nozzle contours and that no additional losses are introduced in the system. The corresponding design/manufacture/assembly tools can be used to a provide low-cost/low-weight controllable propulsion systems to the small-satellite industry with no efficiency loss.

Introduction to Cold-Gas Thrusters

Background

During the last decades, there has been great development of the small-satellite industry due to these sattelites' low manufacturing cost and shorter development time compared to their larger counterparts. Also, orbiting costs are lower as they can be placed as secondary payloads in launcher missions. However, the issue to tackle when building such satellites is miniaturization of components. One key component that presents several miniaturization challenges is the propulsion system (Janson et al. 1999a, b). The term small satellite applies to satellites with masses from less than 1 kg (referred as picosatellites), between 10 and 100 kg (referred as microsatellites), and up to 500 kg (referred as minisatellites).

As it can be seen, there are two orders of magnitude between these categories, which require the use of different technologies for the propulsion system. The different technologies are divided in two groups: high specific impulse–low thrust and low specific impulse–high thrust (NASA 2014). The first group includes electric propulsion technologies such as ion electrospray and Hall thrusters, and the second group includes cold-gas thrusters and rocket motors. In particular, cold-gas thrusters are widely used for small-satellite propulsion, mostly in microsatellites. The main components of a cold-gas thruster are storage tank, pressure regulator, flow valve, and convergent-divergent nozzle. Sometimes, heaters are used to increase the enthalpy of the working fluid, which can be a pressurized or liquefied gas. As tank volume must be minimized, it is desirable to store gas at the highest possible pressure. This increases flow-valve power consumption and requires a pressure regulator to restrain thrust. Moreover, nozzles have to be machined with extremely small throats to further restrain mass flow in order to keep the desired thrust. The same considerations apply for liquefied gas systems, with smaller operating pressures. This has been discussed by several researchers in reviews and thruster specifications, which are given in Janson et al. (1999a, b), Gibbon (2004), Usbeck et al. (2004), CU Aerospace (2014), Matticari (2009), and Louisos and Hitt (2007). All these limitations lead to the conclusion that current cold-gas technologies have low functionality density as many components are required for the proper operation of the thruster, increasing the power, volume, and mass of the system. Thus, cold-gas thrusters must evolve towards solutions with higher functionality density. To illustrate the discussed limitations, Table 1 lists some relevant thruster technologies used in several missions.

It is seen that pressure-control systems are used with pressurized gas to reduce pressure around two orders of magnitude. In all the cases, nozzle throat sizes are in the micromillimeter scale for thrust ranging from 1 to 100 mN. These nozzles have been machined using electroerosion (Matticari 2009), MEMS techniques [such as electrochemical etching (Bayt et al. 1997; Grisnik et al. 1987; Rossi et al. 2006)], or even special lathe machining. In axis-symmetrical nozzles, the machining process is expensive and it is difficult to the control of the internal geometry and surface roughness (Louisos and Hitt 2007). Manufacturing uncertainties cause mass-flow estimation errors that affect mission design. Also, rough surfaces can produce shocks that increase internal nozzle pressure, lowering the specific impulse (Bayt et al. 1997). For these reasons, systems with axisymmetric nozzles need to be extensively tested before launching, increasing mission preparation time.

Concept Description

To increase the functionality density of cold-gas systems, the design of a planar controllable nozzle is proposed. This type of nozzle condenses mass-flow control and thrust production in a single unit with nozzle throat-size and contour-shape design freedom. The features and design characteristics of the proposed planar

[1]Project Engineer, Dept. de Ingeniería Mecánica, Instituto Tecnológico de Buenos Aires, Laboratorio de Energía, Ave. E. Madero 399, C1106ACD Buenos Aires, Argentina. E-mail: ppedreir@itba.edu.ar

[2]Professor of Mechanical Engineering, Instituto Tecnológico de Buenos Aires Dept. de Ingeniería Mecánica, Laboratorio de Energía, Ave. E. Madero 399, C1106ACD Buenos Aires, Argentina. E-mail: rlaure@itba.edu.ar

[3]Head, Dept. of Mechanical Engineering and Computational Mechanics Center, Instituto Tecnológico de Buenos Aires, Ave. E. Madero 399, C1106ACD Buenos Aires, Argentina (corresponding author). E-mail: sdhers@itba.edu.ar

Table 1. Cold-Gas Thrusters Technologies; Approximate Nozzle Size Indicated when Exact Value Was Unavailable

Reference	Nozzle type	Throat	Thrust	Working fluid	Nozzle pressure	Tank pressure
SSTL (Gibbon 2004)	Conical	0.42mm	30–60 mN	Xenon	1–4 bar	105 bar
SNAP-1 (Gibbon 2004)	Contoured	μm-mm	45–120 mN	Butane	4 bar	Liquid
CGS3 (Usbeck et al. 2004)	n/a	μm-mm	0.5–40 mN	N2	0.5–2 bar	200–300 bar
PUC-SO2 (CU Aerospace/Vacco 2014)	n/a	μm-mm	5 mN	SO2	1 bar	Liquid
Galileo-Galilei (Matticari 2009)	Contoured	μm-mm	1–500 μN	N2	1–2 bar	300 bar
Small GEO	Contoured	μm-mm	50 mN	Xenon	2.2 bar	n/a
Moog 58E142 (Bzibziak 2000)	n/a	μm-mm	12 mN	N2	6.9 bar	up to 100 bar
Marotta RJ thruster (Smith 2006)	n/a	μm-mm	50 mN	N2, Xenon, etc.	10 bar	Liquid
TG1 (Omnidea-RTG 2014)	n/a	μm-mm	10–1,000 mN	Inert gasses	5.2 bar	n/a
Rafael cold-gas RCS (Adler et al. 2005)	n/a	n/a	800 mN	N2	15.5 bar	473 bar

controllable nozzle will be given in subsequent subsections (Pedreira et al. 2015).

Nozzle Machining and Contour Design

Planar nozzles can be machined from metal sheets using laser or water-jet techniques at very low cost with any desired surface finish and, specifically when low thrusts are required, the nozzle throat is set through sheet thickness selection.

Since thrust depends heavily on mass flow, the throat section, temperature, and pressure are of primary concern, as seen in the equation for chocked mass flow in a nozzle (Shapiro 1953)

$$\dot{m} \propto \frac{S_T P_0}{\sqrt{T_0}}$$

As temperature has a maximum operational value due to gas decomposition, material properties, and energy requirements, the throat area has to be greatly reduced to keep thrust in the desired range (Bayt et al. 1997). In axis-symmetric nozzles, only the throat radius can be reduced but both throat height and nozzle sheet thickness can be reduced in a planar nozzle. Unlike the case of an axis-symmetric nozzle, this section reduction has a negligible effect on machining costs.

To devise the nozzle's contour, efficient design methods as method of characteristics (MOC), thrust-optimized contoured nozzles (TOC), truncated ideal contoured nozzles (TIC), or parabolic bell nozzles (TOP) can be implemented to maximize a specific impulse (Östlund 2002).

Planar nozzle systems have tighter assembling constraints than axis-symmetric nozzle ones as several parts have to be integrated to build it, which can cause thrust misalignment. This work proposes a functional nozzle design to ensure successful planar nozzle assembly.

For a given expansion ratio, a planar nozzle is longer than an axis-symmetric one. Thus, boundary layer growth can be expected, which could hamper nozzle performance. Furthermore, the wall–fluid contact area is larger, causing high shear stresses that reduce flow exit velocity and thrust. In the case of extremely thin nozzles, boundary-layer growth could choke flow completely.

The aim of this paper is to investigate design tools for planar nozzles, using the method of characteristics (MOC) for design, computational fluid dynamics techniques for a more-detailed calculation, and experimental tests for model correction and validation. Tests are performed in a vacuum chamber under different working conditions. With this set of tools properly adjusted in the range of requirements for microsatellites and nanosatellites, it can be determined whether boundary-layer effects are significant or not. In the present work, 2-mm-thick nozzles are adopted to obtain a suitable thrust range.

Mass Flow and Thrust Control

The proposed mechanism for thrust control separates the nozzle's sides from each other through an actuation system, as shown in Fig. 1. This modifies the nozzle throat area and expansion ratio in a rather simple fashion, providing real-time mass flow and thrust control. A variable nozzle configuration also allows operation under different supply pressures due to gradual empting of the gas tank or due to lack of power for tank heating, saving energy needed for pressure control (heaters, pressure regulators, etc.) and reducing satellite components such as pressure regulators. Overall system efficiency is improved due to the absence of pressure-regulator irreversibilities. The off-design effect on nozzle operation is investigated to determine the h range in which the device has acceptable performance. The actuation system is the only added component. The new system's reliability has to be evaluated for new failure modes not present in axisymmetric nozzles.

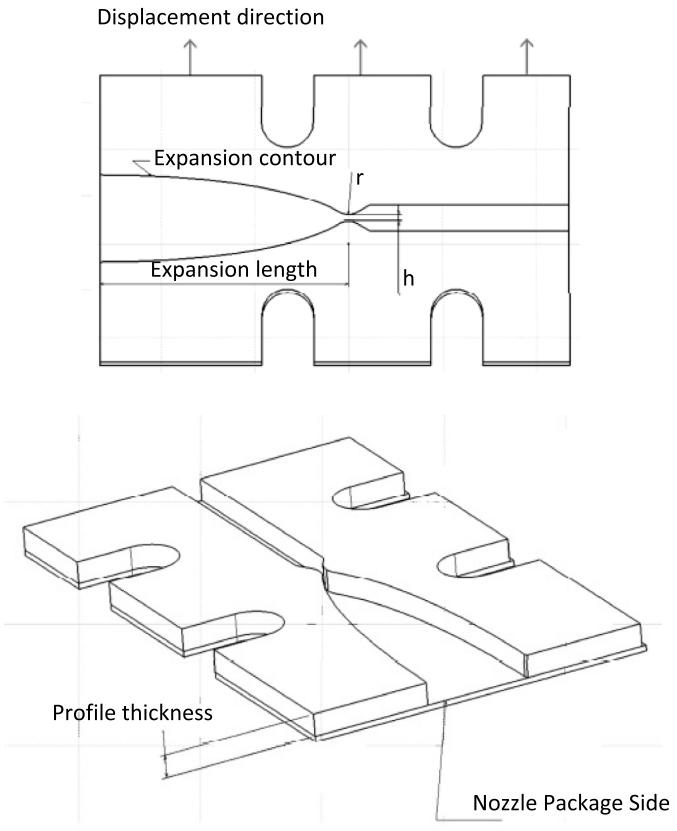

Fig. 1. Nozzle profile and package

Design Procedure and Validation

Nozzle Design

For the experimental and computational work, the nozzle profile is designed with an algorithm based on the method of characteristics (Shapiro 1953; Anderson 2003) initialized with a flow field from a power-series expansion, centered in the nozzle throat, given by Kliegel and Quan (1966) targeted for Mach 4.41 at the exit section. The estimated Reynolds number ranges between 2 10^3 and 4 10^4 under test conditions.

Nozzle Machining (Method and Cost)

Standard-quality laser cutting is a low-cost manufacturing method. The nozzle is cut by a standard supplier who cut several profiles and profile packages in a single operation and out of a single steel sheet. For these reasons, the manufacturing cost less than 5% of that for a conical axis-symmetric nozzle of the same size, expansion ratio, and material is achieved.

The nozzle contour is built as two separate parts in order to check the contour quality using a profile projector. The comparison shows an excellent agreement between the machined and designed contour and repeatability. The nozzle profile is integrated with a laser-cut, mirror-finished container package that ensures parallelism between sheets. The nozzle throat is set using a calibrated wire. Finally, the device's gastight capacity is checked with air up to 7 bar. Fig. 2 shows a scheme of the nozzle and load-cell mounting.

Test Bench

Tests are performed in vacuum chamber. The vacuum is obtained using a two-stage, oil-sealed vacuum pump. Total pressure between 70 and 500 Pa is set for the experiments. The test bench has vacuum and temperature sensors, a hot wire mass-flow meter, stagnation temperature and pressure sensors, and a load cell for thrust measurement. Gas (air) pressure is controlled with a manual pressure regulator. Tests are carried at the desired outlet (vacuum) and inlet pressures opening the solenoid valve for a few seconds. This process is repeated for each nozzle, for a range of inlet pressures.

Computational Fluid Dynamics Modeling

Two computational fluid dynamics (CFD) (*ANSYS*; Majumdar 1988; Raw 1996) models are developed to incorporate into the analysis the boundary layer effects that MOC cannot capture. For optimum convergence rate and reduced computational time, unsteady RANS equations are solved (Otobe et al. 2008; Anderson 1995). The two models are implemented using *ANSYS* CFX commercial software. This package uses the finite-volume method for the discretization of continuity, momentum, and energy equations, combined with the finite-element method. For both models, the discretization schemes are selected as follows. The advection term is solved using a high-resolution scheme (Jasak et al. 1999), which implements an algorithm that is Total Variation Diminishing to keep the solution bounded. Diffusion and pressure gradient terms are solved using a finite-element approach. For the advection term of the turbulence transport equation (Wilcox 1986), an upwind scheme is used.

The models are

- 2D without boundary layer; and
- 2D with boundary layer.

The 2D without boundary layer model has the least computational cost and is used to solve the nozzle flow without boundary-layer effects. It is used to validate the overall accuracy of the nozzle's inner mesh, comparing the results against MOC calculations, which are exact for the Euler equations for compressible flow. Also, if boundary-layer effects are negligible, correct estimations of thrust and mass flow can be obtained.

The 2D with boundary layer model is developed to study the boundary-layer effect on the nozzle contour. Of primary concern are the boundary layer's displacement thickness and growth effect on mass flow (Kim et al. 2005) and flow expansion. Experimental work on axis-symmetrical nozzles (Grisnik et al. 1987) have shown that viscous effects start to reduce nozzle thrust for Reynolds number below 9 10^3, and even more below 4 10^3, which is in the range of the tests.

Two-Dimensional without Boundary Layer Model

The propellant fluid is modeled using the ideal gas law with constant specific heat ratios

$$P = \rho RT$$

This differs very little from real gas models in the range of temperatures and pressures used (Donaldson 1948; Zebbiche 2011). Total pressure and total temperature were set as inlet conditions. The computational domain, adopted mesh, and boundary conditions used are shown in Fig. 3. At the opening boundaries, open boundary conditions with prescribed static pressure and temperature are used. Along the symmetry plane, symmetry boundary conditions are assumed. For turbulence, the shear-stress transport (SST) k-ω model is adopted (Balabel et al. 2011; Saint-Rose et al. 2012; Neckel and Godhino 2015). Free-slip boundary conditions are applied at the nozzle walls (Otobe et al. 2007).

Two-Dimensional with Boundary Layer Model

To model boundary-layer effects inside the nozzle, no-slip conditions and adiabatic wall options are applied to the nozzle walls, while keeping other boundary conditions as in the previous case. Due to the high Mach number expected in the diverging region of the nozzle, the Van Driest transformation is used for proper

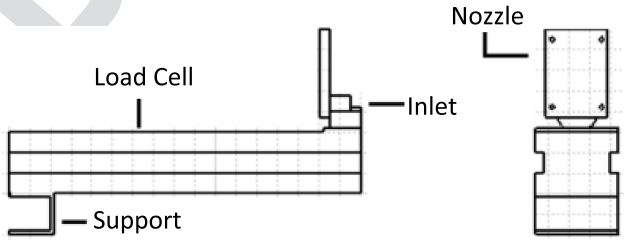

Fig. 2. Nozzle attached to load cell

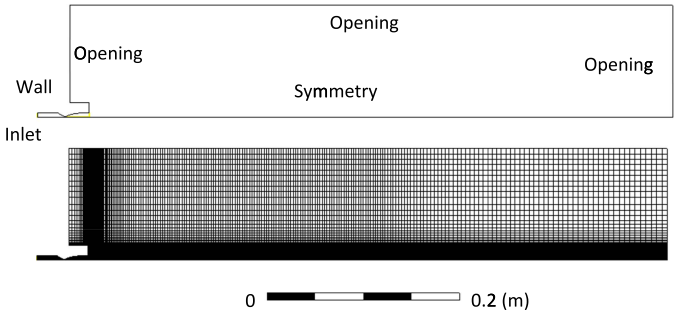

Fig. 3. Computational domain, sample mesh, and boundary conditions

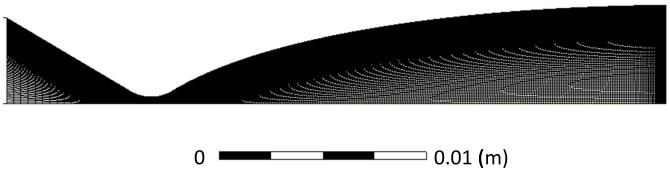

Fig. 4. Detail of nozzle mesh

modeling of boundary-layer growth (Van Driest 1951; Shyy and Krishnamurty 1997).

Mesh Sensitivity

Local mesh density 20 elements thick is placed along the wall, giving a dimensionless wall distance $y+ < 1$ (Schlichting 1979), which is related to the distance from the wall to the contiguous node. Fig. 4 shows a detailed view of the nozzle mesh. The divergent region of the nozzle is chosen for mesh sensitivity analysis, being the region of major interest. Other meshes are constructed keeping the mesh growth ratio below 5% in both mesh directions. The coarsest mesh satisfying these criteria has 8,000 elements in the divergent region. Mass flow, thrust, and axial Mach number distribution are compared to finer meshes of 18,000 and 40,500 elements. As no significant differences were found in any of the calculated values and distributions, the coarser mesh is used for both models.

Results

Validation of MOC and CFD Models

The designed nozzle contour for 4.41 Mach is cut in 2-mm-thick steel with 600-μm throat height. Thrust and mass flow are shown in Figs. 5 and 6, compared to MOC theory and computational values. Good agreement between the different methods can be observed. Chamber pressure is set to match the designed nozzle's exit pressure. In this condition, the thrust equation is

$$T_H = \dot{m} V_{\text{exit}}$$

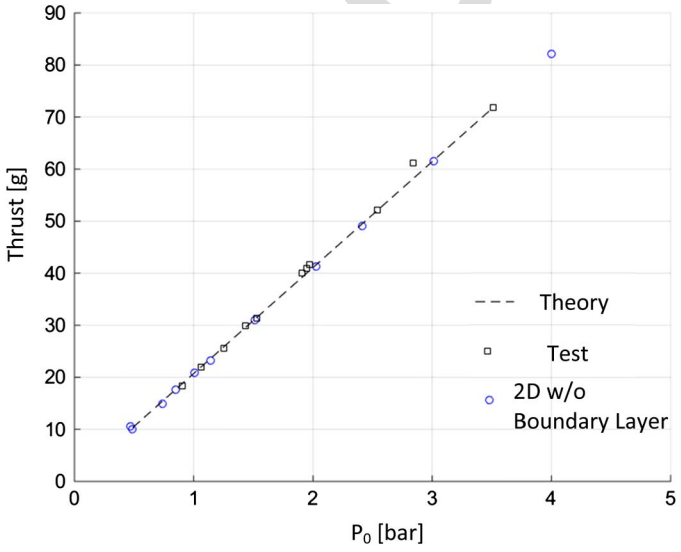

Fig. 5. Thrust for 2-mm-wide nozzle

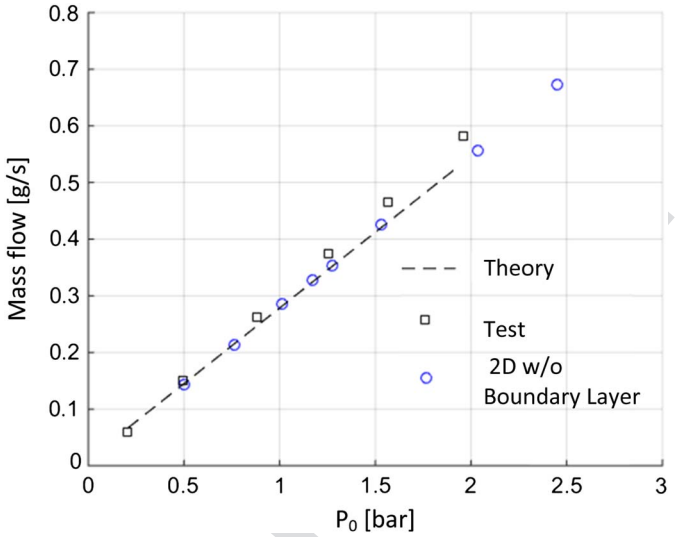

Fig. 6. Mass flow for 2-mm-wide nozzle

As the measured mass flow is very close to the theoretical one, it can be assumed that

$$V_{\text{exit}} \approx V_{\text{theoritcal,exit}}$$

Isentropic efficiency, assuming adiabatic expansion of a nozzle is

$$\eta_{\text{nozzle}} = \frac{\Delta ke}{\Delta ke_s} = \frac{V^2_{\text{exit}}}{V^2_{\text{exit},s}}$$

which in this case is near unity. As thrust is the theoretical one, it can be assumed that flow undergoes a quasi-isentropic expansion; exit velocity is very close to the isentropic one so the process is quasi-reversible. Hence it can be assumed that boundary-layer effects are negligible for the prediction of thrust and mass flow in the proposed range. Thus, properly designed planar nozzles have no efficiency disadvantages compared to axis-symmetrical ones. The computationally predicted design Mach differs only by 0.17% from MOC value (Fig. 7). Furthermore, the computational model shows an almost axial exit velocity distribution, with a slight 1° tilt near the wall as depicted in Fig. 8. This shows that nozzle contour

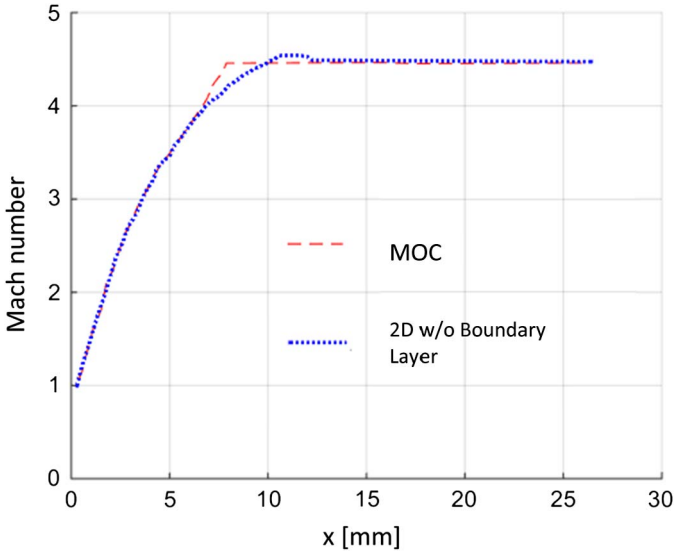

Fig. 7. Axial Mach distribution

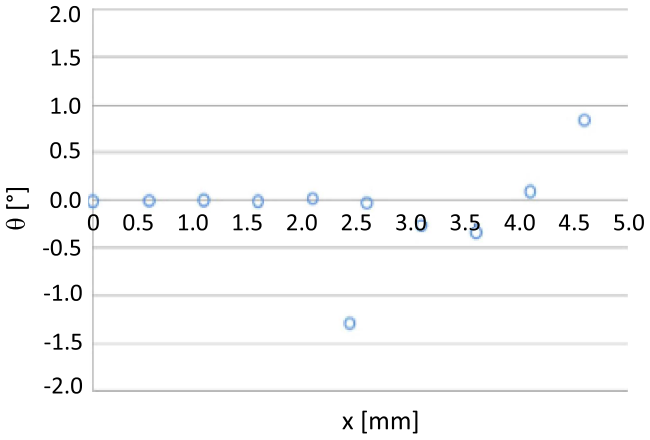

Fig. 8. Flow tilt from axial direction

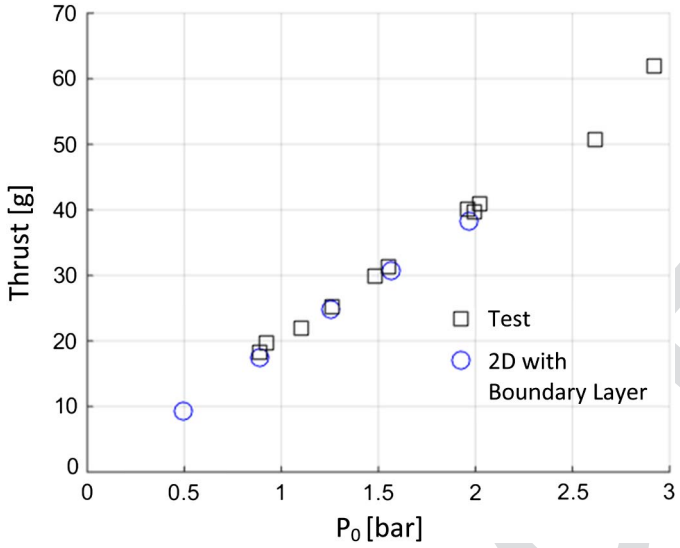

Fig. 9. Thrust for 2D case with boundary layer

effectively guides the flow field in the axial direction, reducing divergence losses.

Boundary-Layer Effects

The 2D with boundary layer model was used to investigate boundary-layer effects along the contour. Figs. 9 and 10 plot obtained thrust and mass flow for the nozzle used in the previous section. Calculated thrust is 4% less than measured thrust, as depicted in Fig. 9. Experimental mass flow is also under predicted 7%. Results are coincident with those from the 2D case without boundary layer model, considering experimental errors. As expected, model shows that the exit Mach reduces along with inlet pressure, due to boundary-layer growth in the expansion zone at lower pressures. This phenomenon is shown in Fig. 11.

To explain how Mach reduction affects nozzle performance, some features of supersonic flows need to be addressed. Mach is defined as

$$M = \frac{V}{\sqrt{kRT}}$$

When a flow expands, changes in Mach are related to an increase in speed and a reduction in temperature. These values

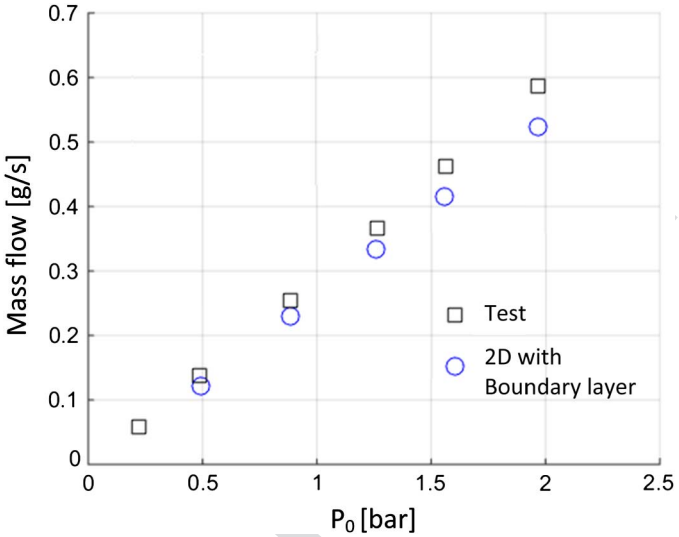

Fig. 10. Mass flow for boundary-layer model

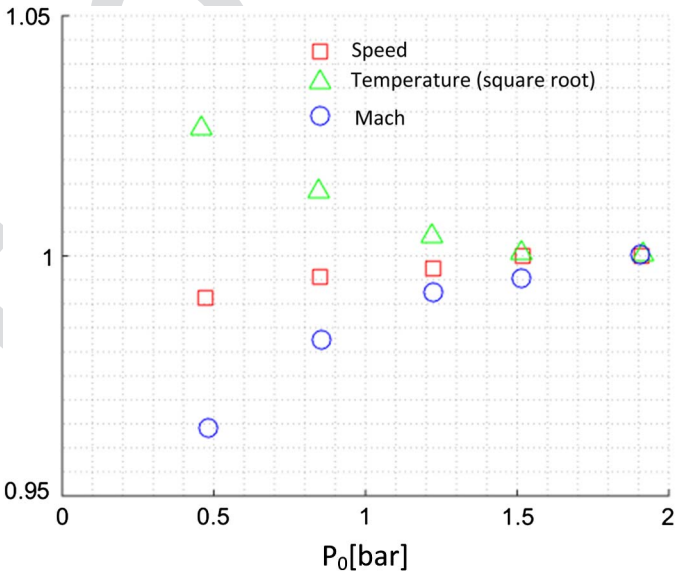

Fig. 11. Exit flow variation; reference values are calculated for highest P_0

change heavily when Mach increases almost up to Mach 3. At this point, flow becomes hypersonic (Shapiro 1953), where changes in Mach are due to changes in flow temperature, with speed remaining almost constant. This phenomenon is observed in Fig. 11 for the MOC designed nozzle, where values are calculated at the exit section's center. Higher temperatures give lower Mach values at constant speeds. This temperature growth is caused by boundary-layer shear stresses. At the lowest studied inlet pressure, exit Mach is 6.6% below design; however exit speed is only 1% lower. In this sense, the designed hypersonic nozzle has an advantage over a supersonic nozzle where Mach is lower, as boundary-layer effects on exit Mach do not hamper the nozzle's performance.

Boundary-layer growth in exhaust section dependence on inlet pressure is shown in Fig. 12, where the velocity profile is plotted against nozzle height. This growth also affects the direction of the flow, turning it outwards the axial direction (Fig. 13). Nevertheless, the tilted flow lies in the boundary layer, which has less momentum and does not add significantly to the total thrust. Fig. 14 shows

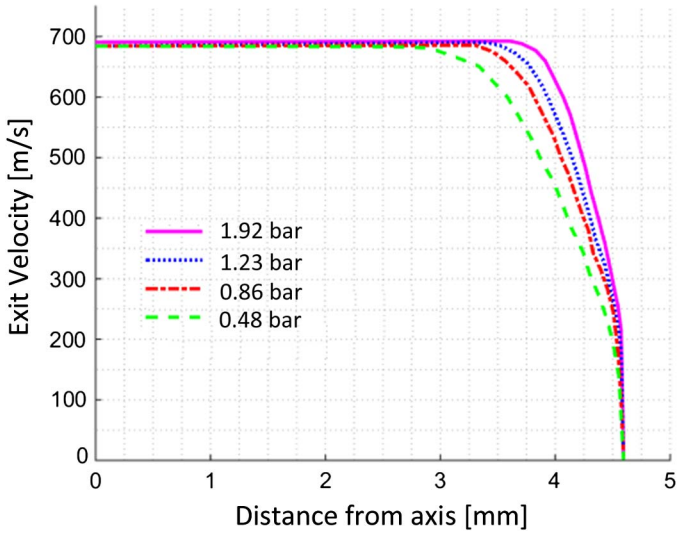

Fig. 12. Velocity profile at nozzle exit

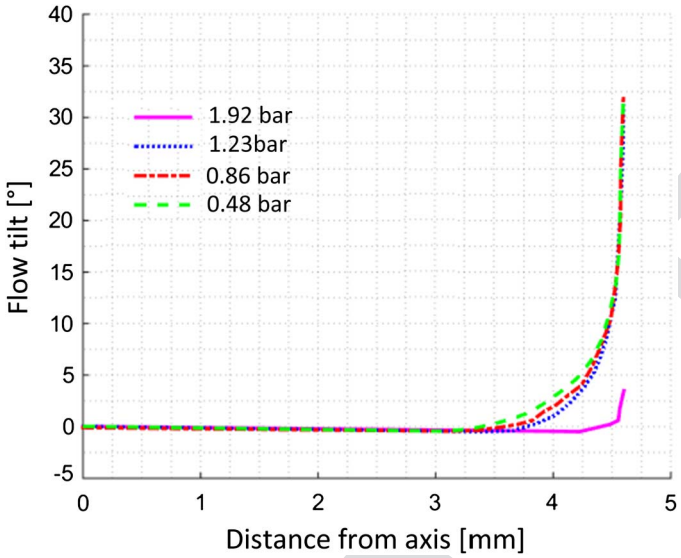

Fig. 13. Deviation of axial direction

boundary-layer development inside the divergent region of the nozzle.

Thrust Control

Planar nozzle side separation can be set as shown in Fig. 1. This setting commands the nozzle throat and consequently the expansion ratio and nozzle profile. The nozzle throat is the key parameter as mass flow depends strongly on it, which allows regulating thrust. Expansion ratio and nozzle profile affect thrust by changing exit Mach and losing flow axiality.

To investigate thrust control capability and performance with a variable throat area, experiments and computational models analysis are carried out. The 2D with boundary layer model is chosen to address the growth of the boundary layer and loss of axiality.

In addition, the MOC design method is enriched to tackle a growing boundary layer. The idea of boundary-layer displacement thickness (Schlichting 1979) is added to MOC code, now named MMOC. Assuming isentropic flow, the boundary layer's displacement is calculated at the nozzle throat in order to fit mass-flow measurements, for a given separation. Then the nozzle profile is offset to get a virtual contour. Standard MOC calculations are performed for the virtual profile and with this correction, thrust is accurately predicted. Results allow concluding that boundary-layer effects for the nozzle can be regarded as a contour offset that reduces the available throat height of the nozzle, without introducing any losses into the system. Results are plotted in Fig. 15. The linear relation between inlet pressure and thrust holds for every tested separation.

Tests also show that the thrust-inlet to pressure ratio is a linear function of the displacement (Fig. 16). This is of paramount importance for controlling the nozzle in an actual system as only two functional parameters have to be specified. In this way, by measuring inlet conditions, the control system can adjust the nozzle step to achieve the desired thrust.

Fig. 15. Variable nozzle; numbers indicate throat height for different displacements

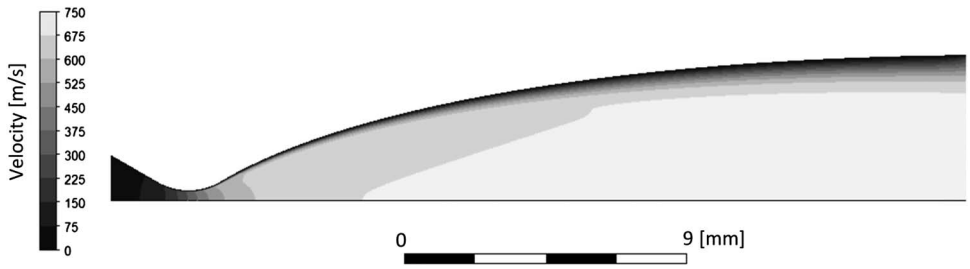

Fig. 14. Boundary-layer development

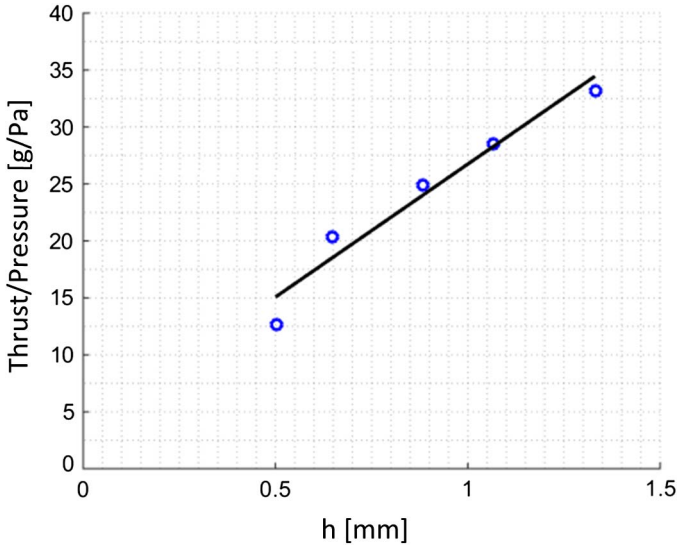

Fig. 16. Nozzle controllability

Conclusions

The small-satellite industry demands thruster technology to evolve to higher functionality densities. Planar nozzles are a fair competitor since miniaturization is possible without performance loss (in this work, nozzles are tested up to 2-mm thicknesses).

The contour boundary layer is found to be small (negligible in most cases) without loss of flow axiality; therefore, no drawbacks arise from the use of planar nozzles compared to the more expensive axis-symmetrical ones. Additionally, real-time thrust control, keeping inlet pressure fixed, can be obtained in a rather simple fashion. The obtained thrust over pressure relation varies linearly with nozzle throat separation, making it easily controllable. In summary for the small-satellites industry, planar laser-cut nozzles have an almost theoretical efficiency at a cost 5% of a similar axis-symmetrical nozzles.

Future work will be focused on designing and testing a controllable nozzle that takes advantage of the conclusion revealed in this work as well as addressing challenging issues such as sealing, robust assembly, and weight reduction in order to offer an alternative to actual axis-symmetrical nozzle-based propulsion systems.

Acknowledgments

The authors would like to thank A. Beceyro Ferran, L. De Cunto, and J. Zapata Usandivaras for their collaboration in the experimental work, Satellogic for their generous donation of the test bench, and Instituto Tecnologico de Buenos Aires for the funding granted through ITBACyT.

Notation

The following symbols are used in this paper:

h = throat height;
Isp = specific impulse;
$\dot{m}$ = mass flow;
M = Mach number;
P = absolute pressure;
R = gas constant;
r = throat radius;
S_T = throat section;
T = temperature;
T_H = thrust;
V = velocity modulus;
Δke = change in kinetic energy;
θ = tilt from nozzle axis;
ρ = density;

Subscripts

0 = stagnation conditions;
exit = conditions at nozzle exit; and
s = isentropic.

References

Adler, S., Warshavsky, A., and Peretz, A. (2005). "Low-cost cold-gas reaction control system for sloshsat FLEVO small satellite." *J. Spacecraft Rockets*, 42(2), 345–351.
Anderson, J. D. (1995). *Computational fluid dynamics: The basics with applications*, McGraw-Hill, New York.
Anderson, J. D. (2003). *Modern compressible fluid flow with historical perspective*, McGraw-Hill, New York.
ANSYS 14.5 [Computer software]. Canonsburg, PA, ANSYS.
Balabel, A., Hegab, A. M., Nasr, M., and El-Behery, S. (2011). "Assessment of turbulence modeling for gas flow in two-dimensional convergent-divergent rocket nozzle." *Appl. Math. Modell.*, 35(7), 3408–3422.
Bayt, R. L., Ayon, A. A., and Breuer, K. S. (1997). "A performance evaluation of MEMS-based micronozzles." *33rd Joint Propulsion Conf. and Exhibit*, Seattle.
Bzibziak, R. (2000). "Update of cold gas propulsion at Moog." *36th AIAA/ASME/SAE/ASEE Joint Propulsion Conf. and Exhibit*, *Las Vegas*.
CU Aerospace/Vacco. (2014). "Propulsion unit for CubeSats PUC-SO2 datasheet."
Donaldson, C. (1948). "Note on the importance of imperfect gas effects and variation of heat capacities on the isentropic flow of gases." NASA, Washington, DC.
Gibbon, D. M. (2004). "Development of a next generation low power small satellite thruster." *Technical Rep.*, Surrey Satellite Technology Ltd, Guildford, U.K.
Grisnik, S. P., Smith, T. A., and Salz, L. E. (1987). "Experimental study of low Reynolds number nozzles." *NASA Technical Memorandum 89858, AIAA-87-0992*.
Janson, S. W., Helvajian, H., and Hansen, W. W. (1999a). "Batch fabricated CW microthrusters for kilogram-class spacecraft." *35th AIIA/ASME/SAE/ASEE Joint Propulsion Conf. and Exhibit*.
Janson, S., Helvajian, H., Hansen, W., and Lodmell, J. (1999b). "Microthrusters for nanosatellites." *2nd Int. Conf. on Integrated Micro Nanotechnology for Space Applications*, Pasadena, CA.
Jasak, K., Weller, H. G., and Gosman, A. D. (1999). "High resolution NVD differencing scheme for arbitrarily unstructured meshes." *Int. J. Numer. Methods Fluids*, 31(2), 431–449.
Kim, J., Kim, H., and Park, K. (2005). "Computational/experimental study of variable critical nozzle flow." *Flow Meas. Instrum.*, 17(2), 81–86.
Kliegel, J., and Quan, V. (1966). "*Convergent-divergent nozzle flow.*" NASA Manned Spacecraft Center.
Louisos, W., and Hitt, D. (2007). "Heat transfer and viscous effects in 2D & 3D micro-400 nozzles." *37th AIAA Fluid Dynamics Conf.*
Majumdar, S. (1988). "Role of underrelaxation in momentum interpolation for calculation of flow with nonstaggered grids." *Numer. Heat Transfer*, 13(1), 125–132
Matticari, G. (2009). "Cold gas microthruster system for Galileo Galilei Spacecraft." *Technical Rep.*, Thales Alenia Space, Cannes, France.
NASA Ames Research Center Mission Design Division Staff. (2013). "Small spacecraft technology state of the art." *NASA/TP–2015–216648/REV1*.

Neckel, A. L., and Godinho, M. (2015). "Influence of geometry on the efficiency of convergent-divergent nozzles applied to Tesla turbines." *Exp. Ther. Fluid Sci.*, 62, 131–140.
Omnidea-RTG. (2014). "Space propulsion components product catalogue."
Östlund, J. (2002). "Flow processes in rocket engine nozzles with focus on flow separation and side loads." M.S. thesis.
Otobe, Y., Kashimura, H., Matsuo, S., Setoguchi, T., and Kim, H. (2008). "Influence of nozzle geometry on the near-field structure of a highly underxpanded sonic jet." *J. Fluids Struct.*, 24(2), 281–293.
Pedreira, P. H., Lauretta, J. R., and D'hers, S. (2015). "Controllable planar nozzles for microthrusters." *1st Pan-American Congress on Computational Mechanics– PANACM 2015*.
Raw, M. J. (1996). "Robustness of coupled algebraic multigrid for the Navier-Stokes equations." *34th Aerospace and Sciences Meeting and Exhibit*.
Rossi, C., Briand, D., Dumonteuil, M., Camps, T., Pham, P., and de Rooij, N. (2006). "Matrix of 10×10 addressed solid propellant microthrusters: Review of the technologies." *Sens. Actuators, A*, 126(1), 241–252.
Sainte-Rose, B., Bertier, N., Deck, S., and Dupoirieux, F. (2012). "Numerical simulations and physical analysis of an over expanded reactive gas flow in a planar nozzle." *Combust. Flame*, 159(9), 2856–2871.
Schlichting, H. (1979). *Boundary-layer theory*, McGraw-Hill, New York.
Shapiro, A. (1953). *The dynamics and thermodynamics of compressible fluid flow*, Ronald Press, New York.
Shyy, W., and Krishnamurty, V. S. (1997). "Compressibility effects in modeling complex turbulent flows." *Prog. Aerosp. Sci.*, 33(9–10), 587–645.
Smith, P. (2006). "Resistojet thruster design and development programme." *42nd AIAA/ASME/SAE/ASEE Joint Propulsion Conf. and Exhibit*.
Usbeck, T., Wohlfart, J., and Schelkle, M. (2004). "A flexible cold gas propulsion system concept for different space applications." *Proc. 4th Int. Spacecraft Propulsion Conf. (ESA SP-555)*, Chia Laguna (Cagliari), Sardinia, Italy.
Van Driest, E. R. (1951). "Turbulent boundary layer in compressible fluids." *J. Aeronaut. Sci.*, 40(6), 1012–1028.
Wilcox, D. C. (1986). "Multiscale model for turbulent flows." *24th AIAA Aerospace Sciences Meeting*.
Zebbiche, T. (2011). "Stagnation temperature effect on the supersonic axisymmetric minimum length nozzle design with application for air." *Adv. Space Res.*, 48(10), 1656–1675.